Antiferromagnet to ferromagnet crossover driven by nonmagnetic Co doping in heavy-fermion $YbRh_3Si_7$

Long Qian,[1] Kelly Neubauer,[2] Joshua Miller,[2] Yuxiang Gao,[2] Jordan Murley,[2] Songxue Chi,[3] Shiming Lei,[2] Pengcheng Dai,[2] and E. Morosan[1,2]

[1]*Department of Chemistry, Rice University, Houston, Texas 77005 USA*

[2]*Department of Physics and Astronomy, Rice University, Houston, Texas 77005 USA*

[3]*Neutron Scattering Division, Oak Ridge National Laboratory, Oak Ridge, Tennessee 37831, USA*

(Received 29 June 2022; revised 20 June 2023; accepted 14 September 2023; published 7 November 2023)

$YbRh_3Si_7$ is a heavy fermion compound that stands out among Yb-based heavy fermions, with its relatively high magnetic ordering temperature and large Yb-Yb distance. To investigate the origin of the magnetic properties in this compound, we synthesized Co doped $YbRh_3Si_7$, achieving a record-high ferromagnetic ordering temperature $T_C = 15.6$ K, only limited by the Co solubility of 20%. Furthermore, we find a crossover from antiferromagnetic to ferromagnetic order with Co doping. The specific heat and magnetotransport measurements show heavy fermion behavior and the persistence of Kondo latticelike behavior in the $Yb(Rh_{1-x}Co_x)_3Si_7$ series.

DOI: 10.1103/PhysRevB.108.184404

I. INTRODUCTION

Heavy fermion (HF) systems are strongly correlated materials on the brink of a magnetic instability. They often exhibit antiferromagnetic order, and can be tuned with external parameters such as magnetic field or pressure. Some known examples are HFs formed with Ce ($4f^1$) or U ($5f^1$) ions [1–5], and much fewer instances of Yb ($4f^{13}$) analogs exist [6–9]. Even fewer ferromagnetic HFs are known, including the Ce-based compounds Ce(Fe,Ru)PO [10], $CeAgSb_2$ [11], $CeRu_2Ge_2$ [12], and one Yb one, $YbNi_4P_2$ [13]. Recently, we reported a new Yb-based HF ferromagnet $YbIr_3Ge_7$ [14], belonging to the class of $ScRh_3Si_7$-type ("137") compounds that also includes two antiferromagnetic HFs, $YbRh_3Si_7$ [15] and $YbIr_3Si_7$ [16]. The three Yb "137" compounds are rare examples of isostructural Yb-based HFs, and one may expect similarities in their physical properties considering their structural similarities and isoelectronic substitutions in going either from Rh to Ir, or from Si to Ge. However, despite the nearly identical lattice parameters, the three compounds have very different ordering temperatures, and drastically different electronic and magnetic properties: the ferromagnet $YbIr_3Ge_7$ and the antiferromagnet $YbRh_3Si_7$ display the expected correlation peak in a metallic resistivity, a common trait of Kondo metals. However, $YbIr_3Si_7$ stands out because of its highly insulating behavior, even though the Hall measurements and band structure calculations indicate the absence of a band gap.

Among the Yb-based Kondo compounds, the three Yb "137" systems appear to have the largest Yb-Yb bond length $d_{Yb-Yb} \sim 5.5$ Å (Fig. 1). Yet, the magnetic ordering temperatures, ranging from 2.4 K for $YbIr_3Ge_7$ to 7.5 K for $YbRh_3Si_7$, are consistently higher than many other Yb-based compounds. This phenomenon is in contrast to the general trend where T_{ord} decreases with d_{Yb-Yb}, as indicated by the clustering in the low T or low d regime of the d-T phase space (Fig. 1). It is therefore remarkable that $YbRh_3Si_7$ orders at a high $T_N \sim 7.5$ K (blue triangle, Fig. 1), much higher than that of closer-packed Kondo systems (with $d_{Yb\text{-}Yb} < 3.6$ Å). Here we report that the ordering temperature in $YbRh_3Si_7$ can be doubled by partially substituting Rh with nonmagnetic Co to form $Yb(Rh_{1-x}Co_x)_3Si_7$ (orange triangles, Fig. 1). Additionally, a crossover from antiferro to ferromagnetic order occurs for $0.09 < x < 0.21$, such that $Yb(Rh_{0.8}Co_{0.2})_3Si_7$ is found to have a ferromagnetic ordering temperature at $T_C = 15.6$ K, second only to that in $\alpha YbAlB_4$ doped with Mn [41]. We demonstrate that Co is not magnetic in $Yb(Rh_{1-x}Co_x)_3Si_7$, and that the Co-doped $YbRh_3Si_7$ remain strongly correlated up to the Co solubility limit $x = 0.2$. These findings underscore the complex interplay between the competing energy scales: Ruderman-Kittel-Kasuya-Yosida (RKKY), crystal electric field (CEF), and Kondo effect, which was recently emphasized in the comparison across the RRh_3Si_7 series [50]. However, when fixing the rare earth to $R =$ Yb and performing substitutions on the nonmagnetic sublattice in $Yb(Rh_{1-x}Co_x)_3Si_7$, RKKY and CEF change very little (with negligible change in d_{Yb-Yb}), while the Kondo scale would be most vulnerable to the Co substitution for Rh [51]. Understanding the origin of the enhanced ordering temperature in this Yb Kondo ferromagnet may offer a pathway to the elusive superconductivity in Yb HFs, if the unconventional superconducting temperature were commensurate with the underlying magnetic correlation scale.

II. METHODS

Single crystals of $Yb(Rh_{1-x}Co_x)_3Si_7$ have been synthesized via the flux-grown method using Rh-Si flux with a similar synthesis condition as $YbRh_3Si_7$ [15]. The composition of the resulting crystals has been identified as $Yb(Rh_{1-x}Co_x)_3Si_7$, with $x = 0.09$, 0.15, and 0.2. For reference, we also synthesized polycrystalline nonmagnetic analogs $Lu(Rh_{1-x}Co_x)_3Si_7$, with $x = 0.03$, 0.14, 0.24, 0.32, and 0.46.

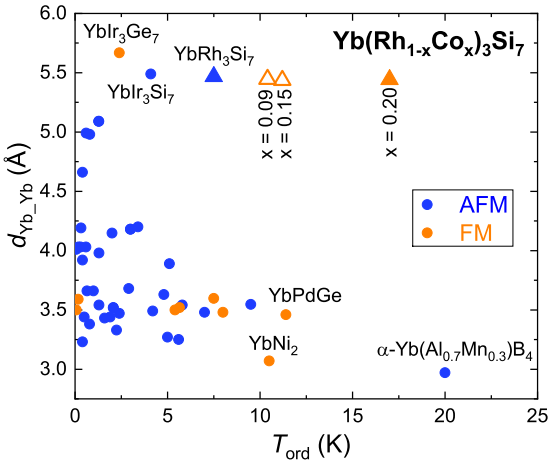

FIG. 1. Yb-Yb distance vs T_{ord} of Yb-based heavy fermions [6–9,13–49].

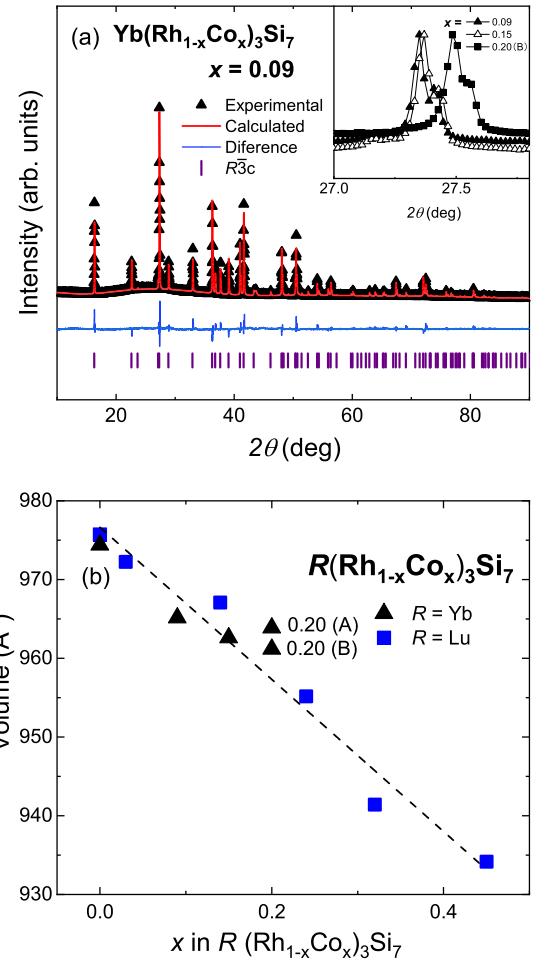

FIG. 2. (a) XRD diffraction pattern for $Yb(Rh_{0.91}Co_{0.09})_3Si_7$. Inset: the (0,0,6) peak for different compositions. (b) Unit cell volume vs x for $R(Rh_{1-x}Co_x)_3Si_7$, R = Yb (triangles), Lu (squares).

Powder x-ray diffraction (XRD) measurements were performed in a Bruker D8 diffractometer with Cu Kα radiation. The Rietveld structural refinement was performed using the TOPAS software. Quantitative analysis by wave length dispersive x-ray spectrometry (WDS) of $Yb(Rh_{(1-x)}Co_x)_3Si_7$ phases was performed via electron probe microanalysis (EPMA), using a JEOL JXA 8530F hyperprobe equipped with a field emission (Schottky) emitter and five WDS spectrometers. The analytical conditions used were 15 kV accelerating voltage, 20 nA beam current, spot beam size (~300 nm). The standard used for Rh, Yb, and Si element calibration was $YbRh_3Si_7$ grown by flux method (same recipe from our previous paper [15]), whereas for Co the pure Co metal was used. Careful background offsets were selected in order to avoid interference with other x-rays during peak and background measurements. The Co percentage in $Lu(Rh_{(1-x)}Co_x)_3Si_7$ was determined by energy-dispersive x-ray spectroscopy (EDX). DC magnetization measurements were performed in a quantum design magnetic property measurement system (QD MPMS) with a ^{3}He option. Specific heat measurements were carried out in a QD physical property measurement system (PPMS) with a ^{3}He option. Resistivity was measured in a four-point contact geometry in a quantum design dynacool PPMS with electrical transport option using AC current with frequency of 9.1 Hz and driving amplitude of 1 mA. The elastic neutron scattering measurements on $Yb(Rh_{0.8}Co_{0.2})_3Si_7$ were carried out on HB3 triple-axis spectrometer at the high flux isotope reactor (HFIR) at Oak Ridge National Laboratory. Pyrolytic graphite monochromators, analyzers, and filters were employed. The incident and final neutron energy was fixed at 14.7 meV. Horizontal beam collimation of open-48'-40'-sample-40-120' was used. The crystal was aligned in the (H, 0, L) scattering plane and was loaded in a closed-cycle cryostat with a base temperature of 4 K.

III. RESULTS

A. Structure and composition

Powder XRD data indicate that the $R\bar{3}c$ rhombohedral structure is preserved for all samples in this study. The unit cell volume decreases with increasing Co content [triangles, Fig. 2(b)] when smaller Co ions partially replace Rh in $Yb(Rh_{1-x}Co_x)_3Si_7$, as expected from Vegard law [52]. A representative powder XRD pattern is shown in Fig. 2(a) for $x = 0.09$, confirming the phase purity at this composition, while the inset shows the (0,0,6) peak shifting with x, confirming the decrease of the c axis parameter as x increases. With a larger amount of Co, increasing amounts of secondary $CoSi_2$ phase can be detected, with the majority phase still being the "137" composition. No magnetism or phase transitions are present in the measurements on pure $CoSi_2$ (not shown), consistent with literature reports that this compound is a Pauli paramagnet [53]. With further confirmation by neutron diffraction measurements for $x = 0.20$, we conclude that the change of magnetic order and ordering temperatures are intrinsic to $Yb(Rh_{1-x}Co_x)_3Si_7$.

Co doping of the nonmagnetic $LuRh_3Si_7$ analog confirms (i) that Co does indeed substitute for Rh and (ii) that Co does not contribute a magnetic moment in these compounds. The Co substitution for Rh is reflected in the linear decrease of the unit cell volume with increasing x (Fig. 2). This decrease in unit cell volume applies chemical pressure to the system and

may have an influence on the magnetic properties, which will be discussed below.

B. Physical properties

$YbRh_3Si_7$ is the first discovered heavy fermion in the "137" class of compounds with an antiferromagnetic ordering temperature $T_N = 7.5$ K [15]. This is higher than that in most known Yb HF compounds (Fig. 1, blue triangle). Upon replacing $4d$ Rh with the $5d$ Ir ion, the resulting $YbIr_3Si_7$ orders antiferromagnetically at a lower temperature, $T_N = 4.1$ K [16], which is still quite high considering the large interatomic distance d_{Yb-Yb} and weak RKKY interactions in Yb HFs (Fig. 1). This observation suggests that the complex interplay between the different energy scales in the YbT_3Si_7 compounds (T = transition metal) can be tuned by the selection of T, and that further enhancement of the ordering temperature is likely with lighter T, such as Co. We therefore study the $Yb(Rh_{1-x}Co_x)_3Si_7$ series, where the Co solubility limit is reached at $x \sim 0.20$.

The low-temperature magnetic susceptibility M/H for $Yb(Rh_{1-x}Co_x)_3Si_7$ single crystals is shown in Fig. 3(a), with the derivatives dM/dT in Fig. 3(b). The composition of two different samples was determined, within error bars, to be $x = 0.20$, and their magnetic susceptibility curves are identified here as 0.2(A) and 0.2(B). The variation in the transition temperature between 0.2(A) and (0.2)B is likely related to the slight difference in their composition. The magnetic ordering temperature T_{ord} is determined as the minimum in dM/dT for each x. The Néel temperature of the parent compound $YbRh_3Si_7$ (down triangles) is 7.5 K, consistent with our prior report [15]. With increasing Co doping, the magnetic transition shifts to higher temperatures, with $T_{ord} \sim 15.6$ K at $x = 0.2$, which nearly doubles that of the parent compound [Fig. 3(b), full and open squares]. Despite the increase in the ordering temperature, the temperature dependence of magnetic susceptibility is similar for $x = 0$ and $x = 0.2$, albeit with much rapid divergence at T_{ord} for $x = 0.20$. Based on the magnetic susceptibility alone, we can determine the value of T_{ord}, but not the type of magnetic transition. Compared to other known Yb HF systems (Fig. 1), the only known compound with a higher ordering temperature at ambient pressure is the Mn-doped $\alpha YbAlB_4$ [49], which has a much smaller Yb-Yb distance (Fig. 1). In this compound, it was concluded that a mixed-valence Yb Kondo lattice was responsible for the high ordering temperature, and Mn doping drove the system closer to a Kondo insulator [41]. This is not the case for the $Yb(Rh_{1-x}Co_x)_3Si_7$ series, where the compounds remain metallic up to the Co solubility limit (see below). Moreover, we show evidence that Co does not contribute to the ordered moment, while the Kondo behavior is preserved up to $x = 0.20$. More importantly, Yb is trivalent throughout the entire doping range, as indicated by the parallel Curie-Weiss linear fits (red lines) in Fig. 3(c).

The $Lu(Rh_{1-x}Co_x)_3Si_7$ compounds (Fig. 4) are nonmagnetic, evidenced by their the small magnetic susceptibility M/H values, nearly temperature-independent as expected for Pauli paramagnets. This indicates that Co does not carry a magnetic moment, and therefore the observed magnetic properties of $Yb(Rh_{1-x}Co_x)_3Si_7$ are solely due to the trivalent Yb ions, while the Co doping might play a role of introducing negative chemical pressure, charge doping, or both. We will revisit the effects of charge doping once the transport properties of $Yb(Rh_{1-x}Co_x)_3Si_7$ are discussed (below).

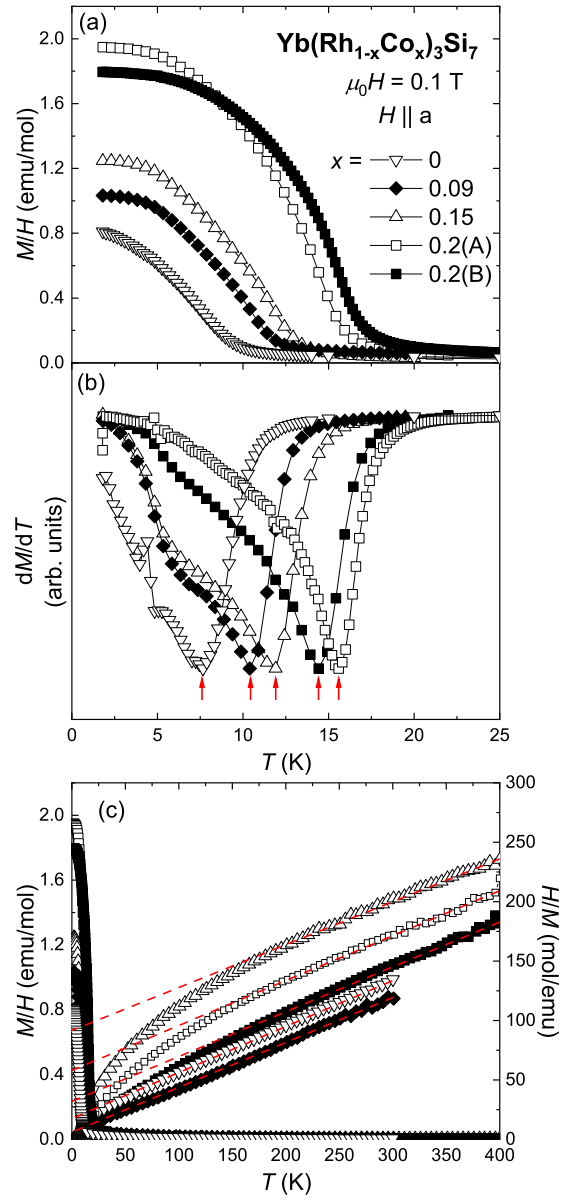

FIG. 3. (a) Low temperature magnetic susceptibility M/H and (b) dM/dT used to determine the ordering temperature T_{ord} (red arrows). (c) Full range magnetic susceptibility M/H (left axis) and inverse magnetic susceptibility H/M (right axis), together with Curie-Weiss fits (red dashed lines) at high temperatures.

We now turn to the specific heat measurements throughout the $Yb(Rh_{1-x}Co_x)_3Si_7$ series up to $x = 0.2$. The ordering temperatures [marked by red arrows in Fig. 5(a)] are consistent with the ones from magnetization measurements, while no sign of phase transition appears in the nonmagnetic $LuRh_3Si_7$ [solid line in Fig. 5(a)]. The C_p/T vs T^2 data for all compositions (black), as well as for the nonmagnetic analog $LuRh_3Si_7$ (blue), are shown in Fig. 5(c). The dotted line is the fit to the high temperature C_p/T vs T^2, which extrapolates to 0.1 J/mol

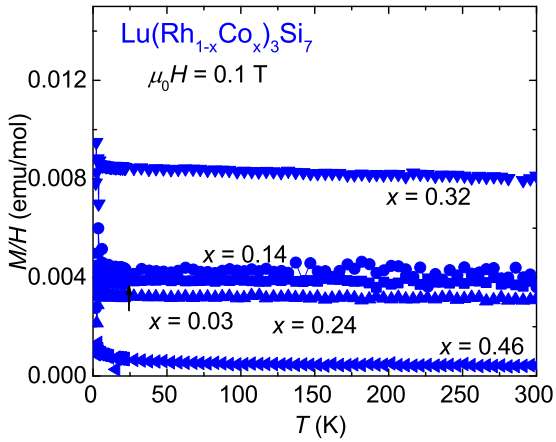

FIG. 4. Temperature-dependent magnetic susceptibility for $Lu(Rh_{1-x}Co_x)_3Si_7$ ($x = 0$, 0.03, 0.14, 0.24, 0.32, and 0.46) under $\mu_0 H = 0.1$ T.

K^2 at $T = 0$. However, this estimate comes from the temperature range above 25 K, which is comparable to the Kondo temperature and close to the highest ordering temperature (for $x = 0.20$). Therefore, a better estimate for the lower limit for γ is given by the dashed line, which extrapolates C_p/T above the magnetic order to $T = 0$, and gives a γ of 0.2 J/mol K^2. The estimated magnetic entropy S_m [Fig. 5(b)] is smaller than R$ln2$ for all these compositions, pointing to Kondo behavior even with Co doping. This point is further reinforced by the resistivity measurements [Fig. 6(a)] for $x = 0$ (triangles), 0.09 (diamonds), and 0.20 (squares). All curves display a broad Kondo coherence peak below ~20 K. This value is consistent with the estimate of T_K from the magnetic entropy as $S_{mag}(0.5T_K) = 0.5\,\mathrm{R}\,ln2$. The resistivity peak extends over a large temperature range. This is likely a consequence of the low carrier density observed in some Kondo lattice compounds, and in the YbT_3M_7 compounds in particular [14–16], as demonstrated by the Hall data (Fig. 8). The resistivity and its temperature dependence of $YbRh_3Si_7$ is similar to that in our prior study [15], where its origin was discussed in detail, and was not related to the magnetic ordering. By contrast, the nonmagnetic analog $LuRh_3Si_7$ (blue line) shows metallic behavior as ρ decreases on cooling. The slightly larger $\rho(T)$ at high temperature for $LuRh_3Si_7$ is likely due to the polycrystalline nature of this sample only, with the resistivity expected to decrease in single crystals, as is the case for the $Yb(Rh_{1-x}Co_x)_3Si_7$ samples.

We have so far established that $Yb(Rh_{1-x}Co_x)_3Si_7$ are HF compounds with unusually high magnetic ordering temperature, which are only surpassed by that of Mn doped α-$YbAlB_4$. However, the "137" compounds (including $YbIr_3Si_7$ [16] and $YbIr_3Ge_7$ [14]) stand out since the high ordering temperature is not a result of enhanced correlation strength commensurate with the interatomic distance, as we discussed above. We therefore aim to understand the nature of the magnetic order, which might provide insight into the responsible mechanism for the enhanced T_{ord}.

We focus on $Yb(Rh_{1-x}Co_x)_3Si_7$ with $x = 0.20$, the compound in this series with the highest ordering temperature $T_{ord} = 15.6$ K. The magnetic order is confirmed by neutron

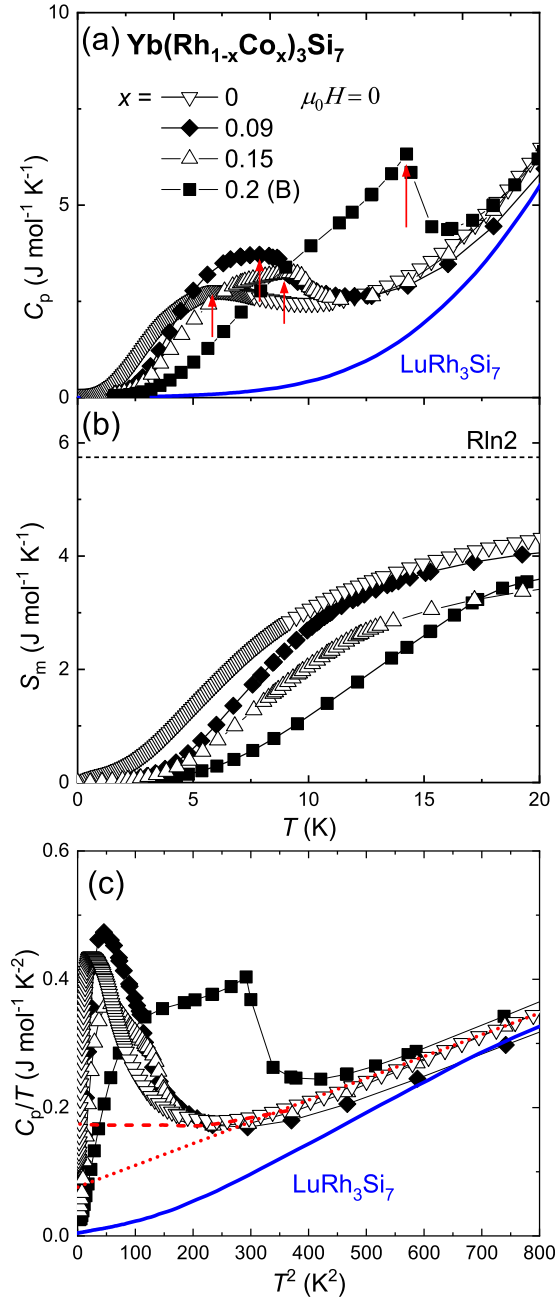

FIG. 5. (a) Specific heat C_p for $Yb(Rh_{1-x}Co_x)_3Si_7$ (scattered symbols) and $LuRh_3Si_7$ (solid line) under zero-field condition. (b) Magnetic entropy S_m for $Yb(Rh_{1-x}Co_x)_3Si_7$. (c) C_p/T *vs.* T^2 for $Yb(Rh_{1-x}Co_x)_3Si_7$ (black, $x = 0$, 0.09, 0.15, and 0.20) and $LuRh_3Si_7$ (blue). Red lines are used for estimating the electronic specific heat coefficient γ at $T = 0$.

diffraction measurements. Figures 7(a)–7(b) shows the magnetic order observed at the FM (0,0,6) reflection (blue) and lack of magnetic order observed at the AFM (0,0,3) reflection (red). The slight deviation from the result in specific heat measurement is mainly due to the thermometer calibration and placement. No discernible intensity gain was observed at indices corresponding to antiferromagnetic (AFM) reflections, indicating that the magnetic structure of $Yb(Rh_{1-x}Co_x)_3Si_7$ with $x = 0.20$ is different than the in-plane AFM order in

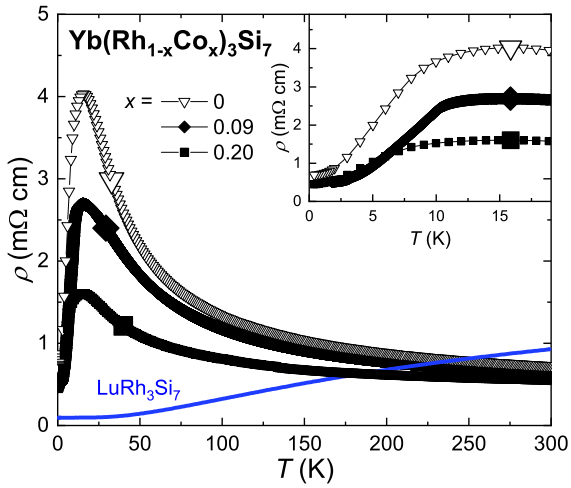

FIG. 6. Temperature dependent resistivity for $Yb(Rh_{1-x}Co_x)_3Si_7$ ($x = 0$, 0.09, and 0.20) under zero-field condition. Inset: low temperature resistivity for Co doped $YbRh_3Si_7$.

the $YbRh_3Si_7$ parent compound [15]. Instead, an in-plane ferromagnetic (FM) structure is expected due to the thermal evolution of the (0,0,6) peak [Fig. 7(e)]. This is indeed consistent with the behavior of the magnetic susceptibility for different applied magnetic fields [Fig. 7(c)]: the susceptibility increases abruptly below T_{ord} (dashed line), and the magnetic transition broadens but does not move in temperature with increasing field. By contrast, neutron diffraction peaks that correspond to antiferromagnetic wave vectors were observed for $x = 0$ [15], where the neutron analysis study showed ferromagnetic (FM) planes stacked antiferromagnetically along the c axis. Co doping in $Yb(Rh_{1-x}Co_x)_3Si_7$ drives a AFM ($x = 0$) to FM ($x = 0.20$) crossover, resulting in a ferromagnetic HF

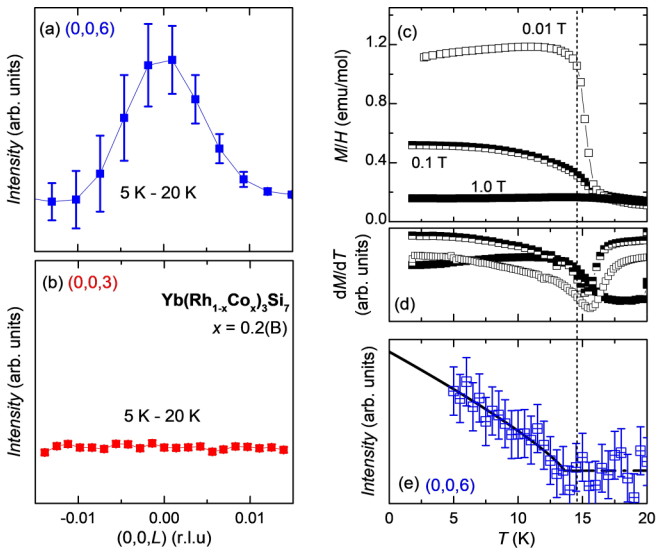

FIG. 7. $Yb(Rh_{1-x}Co_x)_3Si_7$ [$x = 0.20$(B)] Left: Neutron diffraction measurements of the magnetic intensity at (a) (0,0,6) and (b) (0,0,3). Right: the Curie temperature (vertical line) determined from (c) magnetic susceptibility for $\mu_0 H = 0.01$, 0.1, 1 T, the corresponding derivatives (d) dM/dT, and (e) the temperature-dependent neutron diffraction integrated (0,0,6) peak.

behavior in $Yb(Rh_{0.80}Co_{0.20})_3Si_7$, with the second highest magnetic ordering temperature among Yb-based HFs, right next to Mn doped $YbAlB_4$ [41].

IV. DISCUSSION AND CONCLUSIONS

From neutron measurement, the magnetism of the series experience a crossover from antiferromagnetism to ferromagnetism upon Co doping. One possible explanation is the interplay between Co substitution and different energy scales in magnetic ordering: In $YbRh_3Si_7$, the crystal electric field and anisotropic exchange interactions are close to each other in terms of energy between the states with the moment parallel to a and c axes, which is evidenced by the hard axis metamagnetism in $YbRh_3Si_7$ [15]. While the pure sample favors antiferromagnetic order, Co substitution tips the balance and favors the formation of ferromagnetism over antiferromagnetism, while preserving the Kondo physics. With further Co substitution, the applied chemical pressure increases further, and the ordered moments become stronger.

Thermodynamic and transport measurements on $Yb(Rh_{1-x}Co_x)_3Si_7$ indicate an increase of the ordering temperature with increasing Co amounts x. Interestingly, the maximum T_{ord} in this series is not just higher than that

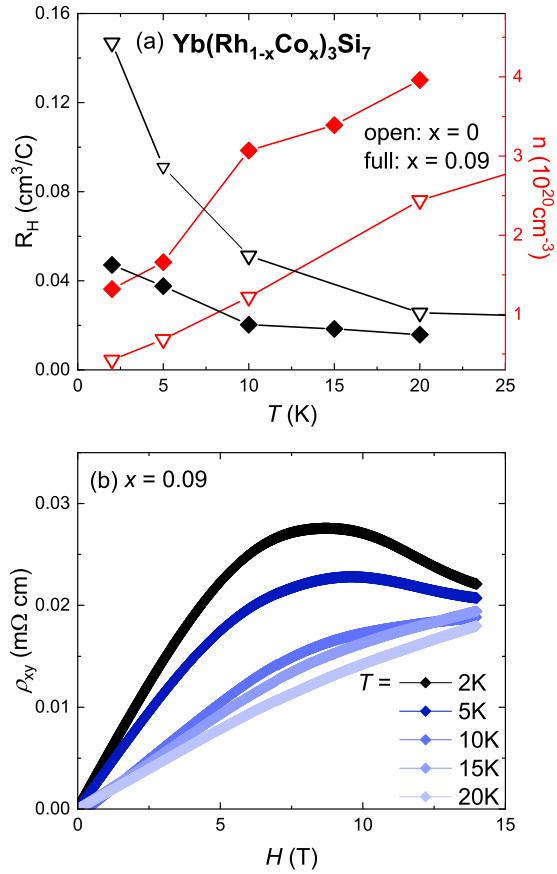

FIG. 8. (a) Calculated carrier density (right axis) and hall coefficient (left axis, black) with a simplified single band model versus temperature. Note that the Hall data measured on $YbRh_3Si_7$ is extracted from from our previous measurement [15]. (b) Hall resistivity of $Yb(Rh_{0.91}Co_{0.09})_3Si_7$ at $T = 2$, 5, 10, 15, and 20 K.

of $YbRh_3Si_7$, but much higher than that of other RRh_3Si_7 (R = Gd-Tm) [50]. Mean field theory predicts de Gennes scaling of the ordering temperature of rare earth compounds in a series, such as in $R_3T_4Sn_4$ (T = Cu, Ag) [54] or R_5Pb_3 [55]. This is not the case in RRh_3Si_7 where the ordering temperature for the Yb compound is the largest even with the lowest $dG = 0.32$ for magnetic R, and Co doping increases the ordering temperature further, to above 15 K.

To date, the Yb-based HF compound with the highest ordering temperature is the Mn doped $\alpha YbAlB_4$ which orders antiferromagnetically at 20 K [41]. For this compound, the magnetic ordering temperature also increases via doping compared to the parent compound. What differs is that the parent compound $\alpha YbAlB_4$ is a paramagnetic Fermi liquid down to 1.8 K [56], while $YbRh_3Si_7$ orders antiferromagnetically at 7.5 K. Also, Mn doping in $\alpha YbAlB_4$ induces a more itinerant moment magnetism, while in Co-doped $YbRh_3Si_7$ the magnetism appears to originate from the local Yb^{3+}, with Kondo screening in the low temperature limit.

It is informative to understand how Co doping changes the dominant carrier contribution in the system, and how this ties into the Kondo picture and the high T_{ord} mechanism. To this end, we performed low temperature Hall measurements, shown in Fig. 8(a) (left axis) for $Yb(Rh_{0.91}Co_{0.09})_3Si_7$ (full) compared with the undoped $YbRh_3Si_7$ (open). We observe the same trend of change with temperature, where the Hall coefficient R_H increases on cooling. In both systems, holes are the dominant carrier type, and the carrier density n derived from a single band picture decreases on cooling from $\sim$20 K to 2 K. This suggests that the $x = 0.09$ Co doping does not change the essential Kondo physics in the $YbRh_3Si_7$ system, although it seems to increase the carrier density. With a closer examination of the field dependence of the Hall data on $Yb(Rh_{0.91}Co_{0.09})_3Si_7$, we observe clear curvature at higher fields [Fig. 8(b)], suggesting the coexistence of electron carriers along with the dominant hole carriers. Compared to $Yb(Rh_{0.91}Co_{0.09})_3Si_7$, the curvature of the field dependent Hall resistivity appears at higher field in $YbRh_3Si_7$ [15]. Overall, these observations suggest that both electrons and holes exist in the undoped and doped systems, consistent with our conclusion that the $x = 0.09$ Co doping does not dramatically change the band structure of the system. Based on our prior band structure calculation results, indeed, two types of carriers are predicted [15].

$Yb(Rh_{1-x}Co_x)_3Si_7$ thus appear as a series of correlated Kondo systems with enhanced magnetic order compared to most known Yb HF compounds. The introduction of Co not only increases the magnetic ordering temperature, but also changes the type of magnetic order. At the same time, the magnetic order occurs at much higher temperatures in these Kondo systems than in the non-Kondo magnetic analogues RRh_3Si_7 [50]. Together, these observations underscore the complex magnetic order in the presence of Kondo correlations in this and the other Yb "137" compounds [14,16].

ACKNOWLEDGMENTS

L.Q., S.L., and E.M. acknowledge support for crystal synthesis and magnetotransport measurements from the Robert A. Welch Foundation Grant No. C-2114; and J.M., J.M., and Y.G. were partially supported by the National Science Foundation Grant NSF DMR 1903741. The use of the EPMA facility at the Department of Earth, Environmental and Planetary Sciences, Rice University, Houston, TX, is kindly acknowledged. The neutron scattering work is supported by the US Department of Energy, Basic Energy Sciences, under Grant No. DE-SC0012311 and in part by the Robert A. Welch Foundation Grant No. C-1839 (P.D.). A portion of this research used resources at the High Flux Isotope Reactor, a DOE Office of Science User Facility operated by the Oak Ridge National Laboratory.

[1] A. Amorese, M. Sundermann, B. Leedahl, A. Marino, D. Takegami, H. Gretarsson, A. Gloskovskii, C. Schlueter, M. W. Haverkort, Y. Huang, M. Szlawska, D. Kaczorowski, S. Ran, M. B. Maple, E. D. Bauer, A. Leithe-Jasper, P. Hansmann, P. Thalmeier, L. H. Tjeng, and A. Severing, Proc. Natl. Acad. Sci. **117**, 30220 (2020).

[2] B. J. Gibson, R. Pöttgen, and R. K. Kremer, Phys. B: Condens. Matter **276–278**, 734 (2000).

[3] D. E. Cox, G. Shirane, S. M. Shapiro, G. Aeppli, Z. Fisk, J. L. Smith, J. Kjems, and H. R. Ott, Phys. Rev. B **33**, 3614 (1986).

[4] E. Yamamoto, Y. Hirose, K. Enoki, K. Mitamura, K. Sugiyama, T. Takeuchi, M. Hagiwara, K. Kindo, Y. Haga, R. Settai, and Y. Ōnuki, J. Phys. Soc. Jpn. **81**, SB023 (2012).

[5] P. Strange and B. L. Gyorffy, J. Phys. F **16**, 2139 (1986).

[6] K. Grube, T. Wolf, P. Adelmann, C. Meingast, and H. v. Löhneysen, Phys. B: Condens. Matter **378–380**, 750 (2006).

[7] A. Oyamada, P. Burlet, L.-P. Regnault, A. Bouvet, R. Calemczuk, J. Rossat-Mignod, T. Suzuki, and T. Kasuya, J. Magn. Magn. Mater. **90–91**, 441 (1990).

[8] K. Katoh, T. Tsutsumi, K. Yamada, G. Terui, Y. Niide, and A. Ochiai, Phys. B: Condens. Matter **369**, 81 (2005).

[9] K. Katoh, Y. Mano, K. Nakano, G. Terui, Y. Niide, and A. Ochiai, J. Magn. Magn. Mater. **268**, 212 (2004).

[10] S. Kitagawa, K. Ishida, T. Nakamura, M. Matoba, and Y. Kamihara, Phys. Rev. Lett. **109**, 227004 (2012).

[11] T. Takeuchi, A. Thamizhavel, T. Okubo, M. Yamada, N. Nakamura, T. Yamamoto, Y. Inada, K. Sugiyama, A. Galatanu, E. Yamamoto, K. Kindo, T. Ebihara, and Y. Ōnuki, Phys. Rev. B **67**, 064403 (2003).

[12] S. Süllow, M. C. Aronson, B. D. Rainford, and P. Haen, Phys. Rev. Lett. **82**, 2963 (1999).

[13] C. Krellner, S. Lausberg, A. Steppke, M. Brando, L. Pedrero, H. Pfau, S. Tencé, H. Rosner, F. Steglich, and C. Geibel, New J. Phys. **13**, 103014 (2011).

[14] B. K. Rai, M. Stavinoha, J. Banda, D. Hafner, K. A. Benavides, D. A. Sokolov, J. Y. Chan, M. Brando, C.-L. Huang, and E. Morosan, Phys. Rev. B **99**, 121109 (2019).

[15] B. K. Rai, S. Chikara, X. Ding, I. W. H. Oswald, R. Schönemann, V. Loganathan, A. M. Hallas, H. B. Cao, M.

Stavinoha, T. Chen, H. Man, S. Carr, J. Singleton, V. Zapf, K. A. Benavides, J. Y. Chan, Q. R. Zhang, D. Rhodes, Y. C. Chiu, L. Balicas, et al., and Phys. Rev. X **8**, 041047 (2018).

[16] M. Stavinoha, C. L. Huang, W. A. Phelan, A. M. Hallas, V. Loganathan, J. W. Lynn, Q. Huang, F. Weickert, V. Zapf, K. R. Larsen, P. D. Sparks, J. C. Eckert, A. B. Puthirath, C. Hooley, A. H. Nevidomskyy, and E. Morosan, arXiv:1908.11336.

[17] D. P. Rojas, J. Rodriguez Fernández, J. Espeso, and J. Gomez Sal, Phys. B: Condens. Matter **404**, 2938 (2009).

[18] C. Schank, G. Olesch, J. Köhler, U. Tegel, U. Klinger, J. Diehl, S. Klimm, G. Sparn, S. Horn, C. Geibel, and F. Steglich, J. Magn. Magn. Mater. **140–144**, 1237 (1995).

[19] S. Ohara, T. Yamashita, Y. Mori, and I. Sakamoto, J. Phys.: Conf. Ser. **273**, 012048 (2011).

[20] P. H. Tobash, Y. Jiang, F. Ronning, C. H. Booth, J. D. Thompson, B. L. Scott, and E. D. Bauer, J. Phys.: Condens. Matter **23**, 086002 (2011).

[21] J. Diehl, H. Davideit, S. Klimm, U. Tegel, C. Geibel, F. Steglich, and S. Horn, Phys. B: Condens. Matter **206–207**, 344 (1995).

[22] P. Gegenwart, J. Custers, C. Geibel, K. Neumaier, T. Tayama, K. Tenya, O. Trovarelli, and F. Steglich, Phys. Rev. Lett. **89**, 056402 (2002).

[23] S. L. Bud'ko, E. Morosan, and P. C. Canfield, Phys. Rev. B **69**, 014415 (2004).

[24] J. Willis, J. Smith, and Z. Fisk, J. Magn. Magn. Mater. **47–48**, 581 (1985).

[25] J. C. P. Klaasse, F. R. de Boer, and P. F. de Châtel, Physica B+C **106**, 178 (1981).

[26] C. Rossel, K. N. Yang, M. B. Maple, Z. Fisk, E. Zirngiebl, and J. D. Thompson, Phys. Rev. B **35**, 1914 (1987).

[27] G. Heinrich, J. P. Kappler, and A. Meyer, Phys. Lett. A **74**, 121 (1979).

[28] R. Pott, W. Boksch, G. Leson, B. Politt, H. Schmidt, A. Freimuth, K. Keulerz, J. Langen, G. Neumann, F. Oster, J. Röhler, U. Walter, P. Weidner, and D. Wohlleben, Phys. Rev. Lett. **54**, 481 (1985).

[29] M. S. Kim, M. Bennett, M. Aronson, J. Millican, and J. Chan, in *APS March Meeting Abstracts, APS Meeting Abstracts* (American Physical Society, 2006) p. K45.001.

[30] P. Bonville, P. Imbert, G. Jehanno, F. Oster, and B. Politt, J. Phys.: Condens. Matter **2**, 4727 (1990).

[31] L. S. Wu, Y. Janssen, C. Marques, M. C. Bennett, M. S. Kim, K. Park, S. Chi, J. W. Lynn, G. Lorusso, G. Biasiol, and M. C. Aronson, Phys. Rev. B **84**, 134409 (2011).

[32] P. Bonville, J. A. Hodges, F. Hulliger, P. Imbert, and H. R. Ott, Mössbauer evidence for magnetic ordering in YbP, in *Anomalous Rare Earths and Actinides*, edited by J. X. Boucherle, J. Flouquet, C. Lacroix, and J. Rossat-Mignod (Elsevier, 1987) pp. 626–628.

[33] K. Hashi, H. Kitazawa, A. Oyamada, and H. Aruga Katori, J. Phys. Soc. Jpn. **70**, 259 (2001).

[34] H. Warring, B. J. Ruck, J. F. McNulty, E.-M. Anton, S. Granville, A. Koo, B. Cowie, and H. J. Trodahl, Phys. Rev. B **90**, 245206 (2014).

[35] C. Engkagul, R. Selim, T. Mihalisin, and P. Schlottmann, Phys. Rev. B **35**, 3686 (1987).

[36] M. Avila, S. Bud'ko, C. Petrovic, R. Ribeiro, P. Canfield, A. Tsvyashchenko, and L. Fomicheva, J. Alloys Compd. **358**, 56 (2003).

[37] B. G. Ueland, A. Kreyssig, E. D. Mun, J. W. Lynn, L. W. Harriger, D. K. Pratt, K. Prokeš, Z. Hüsges, R. Toft-Petersen, S. Sauerbrei, S. M. Saunders, Y. Furukawa, S. L. Bud'ko, R. J. McQueeney, P. C. Canfield, and A. I. Goldman, Phys. Rev. B **99**, 184431 (2019).

[38] S. Lausberg, A. Hannaske, A. Steppke, L. Steinke, T. Gruner, C. Krellner, C. Klingner, M. Brando, C. Geibel, and F. Steglich, arXiv:1210.1345.

[39] W. Miiller, L. S. Wu, M. S. Kim, T. Orvis, J. W. Simonson, M. Gamża, D. M. McNally, C. S. Nelson, G. Ehlers, A. Podlesnyak, J. S. Helton, Y. Zhao, Y. Qiu, J. R. D. Copley, J. W. Lynn, I. Zaliznyak, and M. C. Aronson, Phys. Rev. B **93**, 104419 (2016).

[40] S. Dhar, S. Singh, P. Bonville, C. Mazumdar, P. Manfrinetti, and A. Palenzona, Phys. B: Condens. Matter **312–313**, 846 (2002).

[41] S. Suzuki, K. Takubo, K. Kuga, W. Higemoto, T. U. Ito, T. Tomita, Y. Shimura, Y. Matsumoto, C. Bareille, H. Wadati, S. Shin, and S. Nakatsuji, Phys. Rev. Res. **3**, 023140 (2021).

[42] E. Bauer, R. Hauser, A. Galatanu, H. Michor, G. Hilscher, J. Sereni, M. G. Berisso, P. Pedrazzini, M. Galli, F. Marabelli, and P. Bonville, Phys. Rev. B **60**, 1238 (1999).

[43] K. V. Shah, P. Bonville, P. Manfrinetti, F. Wrubl, and S. K. Dhar, J. Phys.: Condens. Matter **21**, 176001 (2009).

[44] K. Enoki, Y. Hirose, S. Yoshiuchi, K. Sugiyama, F. Honda, T. Takeuchi, E. Yamamoto, Y. Haga, M. Hagiwara, K. Kindo, R. Settai, and Y. Ōnuki, J. Phys. Soc. Jpn. **81**, SB056 (2012).

[45] D.P. Rojas, L. Barquín, C. Echevarria-Bonet, and J. Rodriguez Fernández, Solid State Commun. **152**, 1834 (2012).

[46] N. Tsujii and H. Kitazawa, Solid State Commun. **159**, 65 (2013).

[47] K. Katoh, S. Nakagawa, G. Terui, and A. Ochiai, J. Phys. Soc. Jpn. **78**, 104721(2009).

[48] P. Bonville, P. Bellot, J. A. Hodges, P. Imbert, G. Jéhanno, G. Le Bras, J. Hammann, L. Leylekian, G. Chevrier, P. Thuéry, L. D'Onofrio, A. Hamzic, and A. Barthélémy, Phys. B: Condens. Matter **182**, 105 (1992).

[49] T. Tomita, K. Kuga, Y. Uwatoko, P. Coleman, and S. Nakatsuji, Phys. Procedia **75**, 482 (2015).

[50] L. Qian, S. Lei, B. K. Rai, C. L. Huang, A. M. Hallas, G. T. McCandless, J. Y. Chan, and E. Morosan, Phys. Rev. Mater. **5**, 094416 (2021).

[51] D. Meyers, S. Middey, J. G. Cheng, S. Mukherjee, B. A. Gray, Y. Cao, J. S. Zhou, J. B. Goodenough, Y. Choi, D. Haskel, J. W. Freeland, T. Saha-Dasgupta, and J. Chakhalian, Nat. Commun. **5**, 5818 (2014).

[52] L. Vegard, Z. Phys. **5**, 17 (1921).

[53] D. Shinoda and S. Asanabe, J. Phys. Soc. Jpn. **21**, 555 (1966).

[54] C. J. Voyer, D. H. Ryan, M. Napoletano, and P. Riani, J. Phys.: Condens. Matter **19**, 156209 (2007).

[55] A. Marcinkova, C. de la Cruz, J. Yip, L. L. Zhao, J. K. Wang, E. Svanidze, and E. Morosan, J. Magn. Magn. Mater. **384**, 192 (2015).

[56] R. T. Macaluso, S. Nakatsuji, K. Kuga, E. L. Thomas, Y. Machida, Y. Maeno, Z. Fisk, and J. Y. Chan, Chem. Mater. **19**, 1918 (2007).